Unravelling the physicochemical drivers of heavy metal adsorption on carbonaceous nanomaterials: Implications for the environmental fate of contaminants in mixtures

Mathieu Leroy, Astrid Avellan, Morgan Légnani, Emmanuel Flahaut, Camille Larue

Unravelling the physicochemical drivers of heavy metal adsorption on carbonaceous nanomaterials: implications for the environmental fate of contaminants in mixtures

Mathieu Leroy[a,b], Astrid Avellan[c], Morgan Legnani[b], Emmanuel Flahaut[b], Camille Larue[a*]

[a]Centre de Recherche sur la Biodiversité et l'Environnement (CRBE), Université de Toulouse, CNRS, IRD, Toulouse INP, Université Toulouse 3 – Paul Sabatier (UT3), Toulouse, France, [b]CIRIMAT, Université de Toulouse, CNRS, Université Toulouse 3 - Paul Sabatier, 118 Route de Narbonne, 31062 Toulouse cedex 9 – France, [c]Géosciences Environnement Toulouse (GET), CNRS, Université de Toulouse, 31400 Toulouse, France

*Corresponding author: camille.larue@cnrs.fr; +00-33-(0)5 34-32-37-55

Abstract: The environmental fate of contaminants, particularly nanomaterials, has raised increasing concern due to their potential risks to ecosystems and human health. While adsorption of heavy metals onto carbonaceous nanomaterials (CNMs) has been widely investigated, most studies have focused on single-metal systems, overlooking competitive interactions in mixtures. In addition, many have been conducted under unrealistic CNM/metal ratios and without accounting for metal precipitation, limiting environmental relevance. This study addresses this gap by examining the simultaneous adsorption of Cd, Cu, Pb, and Zn onto CNMs with varying surface properties (surface oxidation, surface area) under environmentally relevant conditions (pH, organic matter content, CNM/metal ratios). Adsorption isotherms show a maximum at neutral pH (13 mmol/g cumulative uptake), with Cu and Pb displaying stronger affinities for oxidized CNM, likely due to metal speciation and interactions with deprotonated functional groups. CNMs with larger surface areas and higher densities of –COOH groups exhibited superior adsorption performance (GO reaching ~29 $mmol \cdot g^{-1}$, i.e. >2× oxidized CNTs). However, increasing organic matter concentrations reduced overall metal adsorption with an 80–100% decrease

for Pb and Cu at 20 mg·L^{-1} OM. Soil solutions with realistic ionic backgrounds did not markedly alter adsorption behavior (3–4 mmol·g^{-1} total adsorption), indicating that pH and CNM surface chemistry remain dominant adsorption drivers. Adsorption kinetics followed a pseudo-second-order model, confirming chemisorption-driven interactions and revealing faster uptake for Cu and Pb than for Cd and Zn. These results highlight the importance of considering multi-metal systems and environmental factors in predicting contaminant fate, providing valuable insights for risk assessment and sustainable remediation strategies. Together, these findings strengthen the foundation needed to anticipate how CNMs reshape metal behavior in real ecosystems.

Keywords: carbon nanotube; surface oxidation; cadmium; copper; lead; zinc

1. Introduction

Human activities lead to an ever-increasing use and environmental release of many contaminants. As such, the fate of contaminant mixtures (cocktail) is a major research topic as interactions among contaminants can modify transfer and toxicity to organisms, making environmental risks more difficult to evaluate. To improve risk assessment strategies, one would need, as a first step, to initiate studies in simplified environments to understand the interactions that occur among contaminants and to identify controlling environmental parameters.

Among contaminants exhibiting strong interaction potential, emerging contaminants such as engineered nanomaterials are of particular interest. Indeed, in recent years, a large diversity of nanomaterials has been investigated for their interactions with contaminants, ranging from inorganic materials studied for adsorption of organic contaminants such as the use of nanohybrids (ZnO/Mo_2TiC_2 MXene) to degrade antibiotic residues[1] or InP_3 monolayers interacting with organochlorine pesticides[2], to biosourced adsorbents—such as cellulose-based biochars - functionalized with MnO_2 or Fe_2O_3 nanoparticles or even amorphous calcium carbonate used to remove dyes or metal ions in single,

binary or ternary systems[3–5]. Beyond these materials, there is an important literature on carbon-based nanomaterials (CNM) such as functionalized carbon nanotubes (CNTs) which could for instance be included in sensing platforms for trace detection of organic molecules[6]. These examples illustrate the growing importance and ubiquity of nanomaterials in environmental contexts.

Another type of contaminant that is particularly relevant in this environmental context is the heavy metal group. They present documented ecotoxicological and human health risks due to their persistence and bioaccumulation. Beyond drinking water, where the World Health Organization (WHO) guideline values are set at 3 $\mu g.L^{-1}$ for Cd, 10 $\mu g.L^{-1}$ for Pb, or 2 $mg.L^{-1}$ for Zn[7], the European Union also regulates maximum levels of heavy metals in food products—for example, 0.020 $mg.kg^{-1}$ Pb and 0.040 $mg.kg^{-1}$ Cd in infant foods[8], highlighting the need to better understand processes governing their environmental transfer and bioavailability. Recent articles also emphasize how chronic exposure to Cd, Pb, Cu and Zn can impair soil microbial communities, plant development and food safety, reinforcing the relevance of studying their environmental fate[9,10].

Furthermore, these two types of contaminants can accumulate and coexist, in particular in agrosystems. Indeed, they tend to accumulate in sewage sludge, which is applied as fertilizer in agrosystems[11] making soil contamination one of the most pressing concerns in the debate about food security and food safety worldwide[12]. In terms of concentrations, models predict that the concentration of CNM in biosolids can reach up to 10 $mg.kg^{-1}$ while in natural soil it remains limited to 0.01 $mg.kg^{-1}$ [13]. Another study calculated that CNT concentrations in European agricultural soils treated with sewage sludge increase annually by 74 $ng.kg^{-1}$ [11]. Additionally, CNT concentration in soil could also increase locally because of their potential application as nanofertilizers[14] or nanopesticides[15], or even as decontamination agent[16]. Concerning metals, they are found in agrosystems for several other reasons such as atmospheric deposition, irrigation with wastewater or polluted water, introduction of livestock manure, metal based-pesticides or herbicides, and phosphate-based fertilizers[17]. Governments decided to regulate heavy metal concentrations by setting maximum allowable

thresholds in agricultural soils up to 1-3, 50-140, 30-75, 50-300, 150-300 and 1-1.5 mg.kg^{-1} for Cd, Cu, Ni, Pb, Zn and Hg, respectively[18]. The interactions between these two types of contaminants, CNM and metals, will likely dictate their fate and bioavailability in agroecosystems and thus possible transfer to the food chain up to humans.

Adsorption of ionic species onto CNM is a complex process, and studies investigating single metal adsorption onto CNM in aqueous media concluded that it is modulated by the CNM properties, the CNM/metal ratio, the contact time and the organic matter (OM) concentration[19–21]. For instance, Langmuir maxima typically reach ~12–36 mg.g^{-1} for Cd, Cu, Pb or Zn on raw CNTs, and increase to ~36–76 mg.g^{-1} on oxidized CNTs. These values highlight how surface chemistry strongly modulates metal affinities (*e.g.* Pb > Cu > Cd for oxidized CNTs)[19]. A recent review highlighted that most studies focused on the adsorption of single metallic ion onto CNM while this type of system is not environmentally relevant as it does not consider the diversity of metals present simultaneously in ecosystems, and their competition for adsorption sites[19]. Indeed, the few articles on that topic highlighted changes when metals were present as a mixture. Ding et al. showed that, at equilibrium, adsorption of Pb, Cu or Ni individually with an adsorbent was decreased when they were added simultaneously[22]. This trend was confirmed in different studies for other metal(loid)s [23–28] so that sequences of affinities can be drawn up and thus highlight different metal affinities for adsorption sites. But with this kind of studies (single metal), the relative affinity of the elements with CNM remains unclear. Only a handful of studies investigated metals in cocktail. For instance, Salam *et al.*[23] reported the following affinity sequence Cu > Zn > Pb > Cd to multi-walled CNT (MWCNT, pH = 7, contact time = 2h, MWCNT = 2500 to 15 000 mg.L^{-1}, ions = 1 mg.L^{-1}) while Sitko *et al.*[26] found Pb>Cu>Cd for graphene oxide (GO, pH = not provided, contact time = not provided, GO = 100 mg.L^{-1}, Cd = 0 to 80 mg.L^{-1}, Cu = 0 to 150 mg.L^{-1}, Pb = 0 to 150 mg.L^{-1}, Zn = 0 to 100 mg.L^{-1}). Likewise, Li *et al.*[27] demonstrated the same sequence (Pb > Cu > Cd) for oxidized-MWCNT (o-MWCNT, pH = 5, contact time = 4H, o-MWCNT = 1000 mg.L^{-1}, ions = 5 to 30 mg.L^{-1}).

However, these studies were carried out with industrial developments in mind, without environmental relevance. In particular, they generally relied on CNM/metal ratios that remain far from environmentally realistic conditions, typically involving large CNM excesses that could lead to a possible metal precipitation and thus an overestimation of adsorption or to a quick saturation of the adsorption sites possibly, modifying affinities and adsorption sequences[29]. As a result, competitive adsorption under field-relevant concentration ratios remains poorly understood. Further, agrosystems are composed of many components which can alter CNM/metal interactions. For example, OM could modify the adsorption of metals[30–32] but the interaction mechanisms among CNM, metals and OM are still unknown. Likewise, only a few studies considered the influence of natural soil solution chemistry, including the presence of competing cations such as Ca^{2+} and Mg^{2+}, which can significantly affect metal–CNM interactions and adsorption equilibria. More studies are needed; since ecotoxicity data available in the literature show either increased or decreased metal(loid) transfer into organisms following CNM addition[19].

The aim of the present work was to bridge these gaps of knowledge by better quantifying competitive metallic sorption onto CNM presenting a variety of binding sites under environmentally relevant conditions. To our knowledge, this study is among the few that explore CNM/metal interactions using ratios that fall within environmentally relevant ranges (approx. ratio of 2500 for Salam *et al*[23], 0.66 for Sitko *et al*[26], 33 for Li *et al*[27], 1.6 for Ding et al.[22] *vs* 0.04 here) allowing more realistic hypotheses about their behavior in natural systems. To do so, we probed the adsorption of ionic metals on carbon-based materials while increasing the medium complexity, studying it on *(i)* oxidized double walled CNT (o-DWCNT) at different environmentally relevant pH, *(ii)* CNM surfaces presenting various functional groups (pristine and oxidized DWCNT, pristine and oxidized-MWCNT, GO, and activated carbon (AC)), and *(iii)* in natural soil solutions. Great care was dedicated to the experimental set-up by including negative controls for each condition to properly account for metal precipitation in the medium under different environmental conditions which is rarely done.

2. Materials and methods

2.1. Materials

CNM synthesis and chemical used

DWCNT, o-DWCNT and o-MWCNT were synthesized at the Centre inter-universitaire de Recherche et d'Ingénierie des Matériaux (CIRIMAT, Toulouse, France). For more details see the supporting information (Figure SI1). Activated Carbon (AC, YPF50), commercial pristine MWCNT (NC3100) and GO were obtained from KURARAY CO., LTD., Nanocyl SA and Antolin Group, respectively.

Stock solutions of Cd(II), Cu(II), Pb(II) and Zn(II) were prepared by dissolving $Cd(NO_3)_2 \cdot 4H_2O$, $Cu(NO_3)_2 \cdot 2.5H_2O$, $Pb(NO_3)_2$ and $Zn(NO_3)_2 \cdot 6H_2O$ (98% purity, Sigma-Aldrich, USA) in ultrapure water.

Soils

Two types of contrasting soils were used. They are standard reference materials from LUFA-Speyer, collected from agricultural sites in Germany and widely used as reference soils in ecotoxicology and soil science. The first one was a loamy sand soil (LUFA-Speyer soil 2.1) sieved to 2 mm with 86.0% sand, 12.6% loam and 1.4% clay. It contained 0.58 wt. % of organic carbon, 0.04 wt. % of nitrogen, with a pH of 5.0 ± 0.1 and a cation exchange capacity of 2.9 ± 0.2 meq.100g^{-1}. The second soil was a clayey soil (LUFA-Speyer soil 6S) sieved to 2 mm with 22.4% of sand, 35.1% of loam and 42.5% of clay. It contained 1.50% of organic carbon, 0.17% of nitrogen, with a pH of 7.3 ± 0.1 and a cation exchange capacity of 18.7 ± 1.2 meq.100g^{-1}. Soil solutions were prepared by adapting the standard AFNOR NF EN 12457-4. Briefly, 100 g of soil were placed in 1 L of ultrapure water, shaken at 180 RPM for 24 hours, centrifuged at 1000 RPM for 2 min (Bioblock Scientific, Sigma 4-15) and then filtered (Merck Millipore, polypropylene, 0.20 µm). Metal content in soil solution was assessed by inductively coupled plasma-atomic emission spectrometry (ICP-AES) and accounted for less than 0.35% of the added metal concentrations (≤ 0.030 mM, Figure S1). Initial pH value of each solution was not adjusted. After preparation, pH of soil solutions was 4.3 ± 0.2 and 5.7 ± 0.2 for LUFA 2.1 and LUFA 6S, respectively. The ionic strength of the two soil solutions was estimated from the elemental concentrations measured by ICP-AES (Table S1), by assuming the dominant ionic forms expected at the measured pH

values. This provides an order-of-magnitude approximation that accounts for coexisting ions likely to influence metal–CNM interactions. The resulting ionic strengths were 0.0026 mol·L^{-1} for soil 2.1 and 0.0047 mol·L^{-1} for soil 6S, which fall within the range expected for agricultural soil extracts.

2.2. CNM characterization techniques

Transmission Electron Microscopy (TEM) was used to assess the diameter of CNMs on at least 20 replicates (JEOL TEM 1400; 120 kV, Centre de microcaractérisation Raimond Castaing, UAR 3623, Toulouse, Figure S2, Table 1). For the length, the measurements provided are a range as the tubes were long and entangled making it impossible to have a reliable precise number. The SSA was determined using the Brunauer-Emmett-Teller (BET) method on one sample as the technique requires a large amount of powder and previous in-house experiments demonstrated the high reproducibility of manufacturer provided batches (Micrometrics Flow Sorb II 2300; 2 h degassing at 100°C in N_2 and adsorption of nitrogen gas at the temperature of liquid nitrogen; measurement accuracy ± 3%; Table 1). Raman characteristics were analyzed to get information on the structural quality (ratio Id/Ig = Intensity of d band/ Intensity of g band) of the CNM used at λ = 633 nm (Labram HR800 Horiba Yvon Jobin; Figure S3 and Table S2). The proportion of carbon and oxygen contained in CNMs was determined with organic micro-analyzers (total combustion at 1050°C under helium/oxygen flux for C and N dosage; total pyrolysis at 1080°C under nitrogen flux for O dosage; SCA CNRS Lyon; Table 1), also on one replicate for the same reason as for BET measurements.

*Table 1: Physico-chemical characteristics (length, diameter, specific surface area and % of C and O) of CNMs (graphene oxide (GO), pristine double-walled CNT (DWCNT), oxidized double-walled CNT (o-DWCNT), pristine MWCNT (MWCNT), oxidized multi-walled CNT (o-MWCNT), and activated carbon (AC)) used in this study. Nd = not determined. Length and diameter/thickness of AC and MWCNT were provided by manufacturing companies. *For GO, its thickness has been determined using the Scherrer equation on the (002) line on the spectrum obtained by XRD (X-ray diffraction)*

Materials	Length (µm)	Diameter/ Thickness (nm)	Specific surface area ($m_2.g^{-1}$)	% of C	% of O
AC	5 to 20	nd	1570	84.6	14.9
DWCNT	1 to 100	2.1 ± 0.7	854	89.7	2.2
MWCNT	< 1.5	10.2 ± 1.1	229	91.8	1.2
GO	0.2 to 8.0	<10*	228	69.0	31.0
o-DWCNT	1 to 100	2.1 ± 0.7	218	76.9	17.2

o-MWCNT	1 to 20	24.2 ± 8.6	60	93.2	6.8

Techniques such as FTIR or SEM/EDS, commonly used for surface characterization, could not be applied here because CNT suspensions cannot be dried or concentrated without inducing agglomeration or altering their surface chemistry. Moreover, the adsorbed quantities of metals in our environmentally relevant exposure conditions (µg–mg range) fall below FTIR and EDS detection limits. This methodological constraint is inherent to studying CNT–metal interactions at realistic concentrations and is acknowledged as a limitation of our study.

2.3. Adsorption experiments

Preliminary tests were conducted to select relevant conditions for adsorption experiments. In order to get closer to environmentally relevant conditions**,** it has been decided to work with metal concentrations in excess compared to CNM adsorption capabilities. *i.e.* 1 mM for each metal and 10 $mg.L^{-1}$ for CNM. Four metals were selected for batch adsorption experiments (Cd, Cu, Pb and Zn: 1 mM with equivalent masses for Cd = 112.41 $mg.L^{-1}$, Cu = 63.54 $mg.L^{-1}$, Pb = 207.2 $mg.L^{-1}$ and Zn = 65.38 $mg.L^{-1}$) due to their toxicity and environmental monitoring. First results showed that metal adsorption was the highest at pH = 7 after 3 hours and these conditions were thus selected for batch adsorptions. To test the effects of CNM characteristics (SSA, diameter, surface oxidation), metal adsorption onto pristine DWCNT, pristine MWCNT (MWCNT), oxidized MWCNT (o-MWCNT), GO and AC were compared to o-DWCNT. To investigate the effect of pH and OM on metal adsorption onto o-DWCNT, relevant environmental conditions were selected with a pH ranging from 5 to 8[33] and two concentrations of OM of 10 and 20 $mg.L^{-1}$[34].

The experimental design was the same for all batch adsorption experiments. Before introducing 50 mL of the metal cocktail solution in an erlenmeyer flask (V = 100 ml), the initial pH values were adjusted to 7 with 10 M NaOH solution. Then, CNM (500 µL, leading to a final concentration 10 $mg.L^{-1}$) were

198 introduced in experimental units (together with OM in one experiment) and the suspensions were
199 placed under shaking on an orbital shaker plate at 200 rpm for 3 hours (except for kinetics experiments)
200 at room temperature (18.3 ± 0.9 °C). Before each experiment, CNM suspensions were sonicated for
201 5 min to ensure reproducible dispersion. Visual inspection showed no visible agglomeration over the
202 3 h adsorption period. This stability was further supported by DLS measurements, which confirmed
203 that the hydrodynamic size distribution of o-DWCNT suspensions remained unchanged throughout the
204 experiment, even though absolute size values are not reliable for non-spherical fibrous materials such
205 as CNTs. Samples were then centrifuged at 4000 rpm (room temperature) for 5 min. Finally, samples
206 were filtered on 0.45 µm polypropylene filtration membrane (LABO MODERNE). All adsorption
207 experiments were conducted with n = 5 replicates per condition. One specificity of this experimental
208 set-up was that control experiments were performed in each case in the absence of CNM as negative
209 controls. Corrected adsorption values were calculated by subtracting metal losses measured in
210 negative controls, allowing us to isolate true adsorption from pH-dependent precipitation processes—
211 a step often omitted in previous studies but essential here given the environmentally relevant pH
212 range. For more clarity, all experimental parameters of each experiment are summarized in Table S3.

213 In preliminary tests, we evaluated additional models (Freundlich, pseudo-first-order). Freundlich
214 showed poorer fits than Langmuir for all metals, and pseudo-first-order kinetics consistently
215 underperformed compared to the pseudo-second-order model. As the Langmuir and pseudo-second-
216 order models provided the most robust and mechanistically consistent description of our system, other
217 empirical models (including Temkin) were not retained.

218 The effect of the ratio o-DWCNT/metal concentration was modelled using the Langmuir isotherm with
219 the following equation (1):

220 $$(1)\ Langmuir:\ q_e = k_L q_m C_e / (1 + k_L C_e)$$

221 where q_e and q_m (mmol.g^{-1}) represent equilibrium and maximum adsorption capacities, respectively;
222 C_e (mmol.L^{-1}) the equilibrium aqueous concentration; k_L (L.mmol^{-1}) the equilibrium constant.

Parameters were fitted using both linear and non-linear regression, and model performance was assessed from R^2 analysis. Here, the Langmuir model was used as a descriptive framework to compare competitive binding among metals rather than to infer strict monolayer mechanistic assumptions. For isotherm modelling, 0.1-4 mM range concentration of Cd and Zn, 0.2-4 mM for Pb and 0.1-2.5 mM for Cu were used due to metal precipitation.

Kinetics experiment was described by diffusion models such as the pseudo-second-order following this equation (2):

$$(2)\ Pseudo\ second\ order:\ q_t = k_2 q_e^2 t/(t k_2 q_e + 1)$$

where q_t and q_e are the adsorption capacities (mmol.g^{-1}) at time t and equilibrium and k_2 (g.mmol.min^{-1}) is the constant rate of the pseudo-second order.

Goodness-of-fit was evaluated using regression statistics and comparison of experimental *vs.* predicted qt values.

2.4. Analytical measurements

After the adsorption experiment, the remaining metals in solution (*ie* not adsorbed on CNM or precipitated in solution) were quantified by inductively coupled plasma – atomic emission spectrometry (ICP-AES) after sample acidification to reach 3% HNO_3 (ARCOS FHX22, AMETEK Spectral).

2.5. Modelling and statistical analyses

Metal speciation in solution at different pH was modeled through Pourbaix diagrams using the software Visual Minteq 3.1.

Langmuir isotherms and diffusion modelling were performed on Microsoft Excel 2019 version 1808.

To account for metal precipitation, the data was normalized thanks to the negative controls (condition with metal but without CNM) as follows (example for Cd):

Cd adsorption for replicate n°1 = mean of Cd concentration of five replicates without CNM - Cd concentration for replicate n°1 with CNM.

Then, adsorption concentrations (mmol.g^{-1}) obtained were corrected with CNM concentration in the sample to obtain for each ion used in experiments: $\frac{\text{ions concentration (mmol)}}{\text{g of CNM}}$.

All statistical analyses were performed using RStudio software (version 3.4.1). First, 1-way ANOVAs were performed on adsorption data to test the effects of each parameter investigated in batch adsorption experiments (metal concentration, pH, contact time, OM concentration, soil solutions). The normality, independence and homoscedasticity of the residuals were checked using Shapiro, Durbin-Watson and Breusch-Pagan tests, respectively. Data were transformed to log or square root if one of the three conditions of validity was not met. A non-parametric Kruskal-Wallis test was performed in case of failed transformations. Significance was set at $p < 0.05$.

3. Results and discussion

3.1. pH influence

First, cumulative metal adsorption onto o-DWCNT increases with pH with a maximum adsorption reached at pH = 7 up to 12.29 mmol.g^{-1}, before decreasing at higher pH = 8 down to 6.28 mmol.g^{-1} (Figure 1, Kruskal-Wallis test among pH conditions, p=0.027). This quantitative data is difficult to compare with the literature as, to the best of our knowledge, our experimental set-up is one of the few trying to get closer to environmental values and thus with metal in excess in comparison to CNM. According to our recent review, the highest adsorption values obtained in mono-elemental systems reached about 4.7 mmol.g^{-1}, 4.6 mmol.g^{-1}, 8.9 mmol.g^{-1} and 5.2 mmol.g^{-1} for Cd, Cu, Pb and Zn,

271 respectively[19]. Likewise, the cumulative adsorption concentrations achieved in multi-metal systems
272 ranged from 0.5 to 5 mmol.g^{-1} [19]. Even though our results are in the same range, they tend to be higher,
273 probably resulting from the ratio metal/CNM; for instance, in the study from Ding et al, the highest
274 metal concentration tested was 0.6 mmol.L^{-1} with a concentration of 200 mg.L^{-1} of carbon nanofibers[22].
275 However, the overall behaviour according to the pH is in agreement with the general trend found in
276 the literature, showing that metal adsorption depends on the solution pH, similarly to what is observed
277 both in single metal systems[26,35,36] and in multi-metallic systems[22,23,27]. In particular, Salam *et al.*
278 highlighted a maximum adsorption for Cu and Pb onto MWCNT at pH = 6, while it was not reached for
279 Cd and Zn in the tested pH range (pH range: 3 to 9)[23]. At higher pH (pH=8), this increase in adsorption
280 was not detected here. This difference is probably related to different experimental set-up as Salam
281 et al. quantified both actual metal adsorption and metal precipitation while we could discriminate
282 thanks to the negative controls set-up here (allowing to subtract metal precipitation from adsorption).
283 Indeed, Minteq modelling suggests metal precipitation at pH=8 (Figure S4) which was further
284 experimentally confirmed at least for Pb (Pb_{pH8}= 0.87 mM in negative control *ie* without o-DWCNT).

285 Second, metals were not adsorbed in the same proportions at the different tested pH. Indeed, two
286 metal adsorption patterns could be defined according to the pH range: (i) in the range pH = 5 to 6,
287 metal adsorption was low (around 1-2 mmol.g^{-1}) and quite similar among metals, and (ii) for higher pH,
288 metal adsorption was higher and metal dependent (more than 5 and 4 mmol.g^{-1} for Cu and Pb,
289 respectively) so that adsorption sequences could be defined at the maximal adsorption pH (pH = 7) as
290 follows: Cu ≈ Pb > Cd ≈ Zn, while it was: Pb > Cu > Cd ≈ Zn at pH = 8.

291 Salam *et al.* obtained a different pattern, where Cu was already more adsorbed than other metals onto
292 MWCNT starting from pH = 5 (Cd, Pb and Zn)[23]. Also, at pH = 7, they highlighted the following sequence:
293 Cu > Zn > Pb > Cd, while Sitko *et al.* found a sequence similar to ours (Pb > Cu > Cd > Zn) with GO[26].

294 Firstly, the nature of the adsorbent itself and the resulting mechanisms of adsorption will modulate
295 the affinities. Indeed, oxidized materials (o-DWCNT and GO) due to the presence of -COOH and -OH

296 groups would favour adsorption based on ionic and electrostatic interactions, while it would be more
297 of a physical nature for pristine materials[16,19,36–39]. Electrostatic interactions (and thus ionic
298 interactions) are highly pH dependent as both CNM and metal forms will evolve with the pH. For CNM,
299 when the pH is higher than their point of zero charge (pH_{PZC}), their overall surface is negatively charged
300 and thus cation adsorption is favoured due to electrostatic interactions while when $pH \leq pH_{PZC}$, cation
301 adsorption is lower due to the neutralization of the surface charges of CNM, or even the presence of
302 repulsive positive charges[19]. The PZC is determined by the quantity and type of functional groups
303 present on CNM surface. In the pH range we investigated, the presence of carboxylic groups will greatly
304 influence metal adsorption. In the literature, the pKa of carboxylic groups at the surface of CNT has
305 been evaluated at 5.1 and 6.4[40]. At these pKa 50% of the carboxylic groups are deprotonated and one
306 can consider that this percentage can reach 90% at a pH higher by one unit. This means that at acidic
307 pH range (pH = 5-6), physisorption would be predominant leading to a low adsorption, and similar
308 among metals. At pH = 7-8, chemisorption becomes predominant favoring metal adsorption on
309 deprotonated carboxylic groups. Similar pH-dependent shifts between physisorption and
310 chemisorption have been reported in other multicomponent adsorption systems, where competing
311 ions or molecules modulate site accessibility and affinity sequences through electrostatic interactions
312 and surface complexation, as observed for mixed-dye systems[5] and for functionalized biomaterials
313 exposed to metal mixtures[4].The affinity sequence highlighted here then relies on the different physico-
314 chemical properties of the ions (Table S4). One important property is the formation constant (Kf): the
315 higher this constant, the more stable the formed complexes are. Two groups can be distinguished: one
316 with Cu and Pb (log(Kf)=18.8 and 18.0, respectively) and one with Zn and Cd (log(Kf)=16.5). Cu is
317 significantly more adsorbed than Pb which might be related to the fact that it has a smaller ionic radius
318 giving it an easier access to adsorption sites in comparison with Pb (0.73 Å *vs* 1.2 Å) as well as a higher
319 charge density (9.7 C/m^3 *vs* 3.7 C/m^3) leading to stronger electrostatic interactions. Electronegativity
320 could also partly explain that ranking (Tables S3) but seems to be playing a secondary role.

Finally, as mentioned above, the pH also conditions metal forms in solution with lower pH being more favourable to ionic forms while higher pH leads to precipitation - but this phenomenon is element dependent (Figure S4 and S5). It could explain the change in the affinity sequence detected at pH=8 as the modelling suggests the presence of more Pb soluble species than Cu soluble species at this pH.

In this work, it thus seems like the sequence of affinities and its change with pH can be explained by the pH-dependent deprotonation of binding sites, the intrinsic properties of ions, along with their metallic speciation in water evolving towards precipitation for higher pH.

Regarding the median value of pH in agricultural soils in Europe (pH = 5.8)[41], metals would be weakly adsorbed and in a similar proportion. However, in the environment, and in particular in agrosystems, it has been proven that sewage sludge application (main entry pathway for CNM) increases soil pH to pH=7 or 8[42], which according to our results could reinforce the adsorption of metals on the surface of o-DWCNT. In addition, sewage sludge application also increases metal availability and thus their adsorption behaviour and potential toxicity.

3.2. Isotherms & Kinetics

Non-linear and linear Langmuir isotherm models were applied to simulate and understand the adsorption mechanism of metal ions (Cd(II), Cu(II), Pb(II) and Zn(II)) on o-DWCNT (Figure 2, Figure S6). Due to metal precipitation, the concentration range used to build Langmuir isotherms was selected specifically for each metal.

First, it can be noticed that the sorption isotherms fitted better for Cd(II), Pb(II) and Zn(II) than for Cu(II) as correlation coefficients were *ca.* 0.90 while it was 0.81 for Cu(II) (Figure 2B). This is probably due to the fact that equilibrium was not reached for Cu(II) only in our exposure conditions as it is the first metal that precipitates in the medium (Figure S4, S5). Despite this, the four correlation coefficients and the fit between the Langmuir model and the experimental values were satisfactory (even if initially this model was designed to study the solid/gas interface) as they were higher than 0.80. In mono-

346 metallic systems, the mean R^2 (R^2 = 0.97) of studies reviewed in Leroy *et al.*[19] was higher than in multi-
347 metallic systems, which suggests that metal interactions lead to more variability within the system.

348 According to the linear Langmuir fit (Figure 2A) which allows to establish the value of q_{max} (Figure 2B),
349 we can see that the equilibrium was reached at values close to those indicated by non-linear Langmuir
350 representation for the four metals, which were 16.9, 4.9, 3.4 and 3.3 mmol.g^{-1} for Cu(II), Pb(II), Zn(II)
351 and Cd(II) with the linear model and 14.0, 4.6, 2.1 and 2.1 mmol.g^{-1} for Cu(II), Pb(II), Zn(II) and Cd(II)
352 with the non-linear model (Figure S6). The q_{max} adsorption coincided well with the experimental
353 adsorption (q_{exp}) with q_{exp} up to 13.5, 5.5, 1.5, 1.2 mmol.g^{-1} for Cu(II), Pb(II), Zn(II) and Cu(II),
354 respectively.

355 The separation factor R_L calculated from the Langmuir model, which reveals whether the adsorption is
356 irreversible (R_L = 0), favourable (0< R_L <1), linear (R_L = 1) or unfavourable (R_L >1)[43], indicates that
357 adsorption was favourable for all metals studied. In addition, $K_{L,}$ which corresponds to the extent of
358 the interaction between the adsorbate and the surface where a larger value of K_L, indicates a stronger
359 interaction between the adsorbate and the adsorbent, reveals the following adsorbate/adsorbent
360 interaction sequence Pb>Cd>Cu>Zn. It is the combination of K_L and R_L that establishes q_{max}, hence the
361 adsorption affinity sequence.

362 This affinity sequence confirmed what was already observed in the previous experiment (pH variation
363 with 1 mM metal) and also fits with what we highlighted in mono-metallic systems in our review paper
364 with the following sequence based on q_{max} values for oxidized CNT: Pb(II) > Ni(II) > Cu(II) ≥ Cd(II) > Hg(II)
365 ≥ Cr(II) ≥ Zn(II)[19]. It thus seems that the simultaneous presence of metallic species of different nature
366 in solution does not modify the affinity of metals for the adsorption sites pre-established in mono-
367 metallic systems (at least when the concentrations of the different ions is low or in the same range and
368 in the solubility range).

369 Comparing the limits of metal concentrations in European agricultural soils at the range 6 < pH < 7 (Cd:
370 1-3 mg.kg^{-1}, Cu: 50-140 mg.kg^{-1}, Pb: 50-300 mg.kg^{-1} and Zn: 150-300 mg.kg^{-1})[44] and metal

concentrations in this study at pH = 7 (1 mM of Cd: 112 mg.L^{-1}, 1 mM of Cu: 64 mg.L^{-1}, 1 mM of Pb: 207 mg.L^{-1} and 1 mM of Zn: 65 mg.L^{-1}), it would be expected that the quantities of metals adsorbed on the CNM surface would follow the same order as the affinity sequence defined in our study. However, this forecast is only indicative as many other soil components may interact with both CNM and metals such as aluminium and iron oxide or hydroxide phases, or clays.

To try to go further into adsorption mechanisms, the kinetics of adsorption with pseudo-second order linear plot with t/qt versus time was modelled to deduce some kinetics parameters (Figure 3). First, adsorption kinetics of metal mixtures were well translated by pseudo-second order model as correlation coefficients were > 0.9. Second order rate constant (K_2) was different from metal to metal, reaching 0.37, 0.26, 0.18 and 0.02 g.mmol^{-1}.min^{-1} for Cu(II), Zn(II), Pb(II) and Cd(II), respectively. The metal quantity at the equilibrium (q_e) followed the previously determined order as Cu(II) > Pb(II) > Cd(II) ≥ Zn (II). As seen through the Langmuir isotherm modelling, Pb(II) had a stronger interaction with the surface of o-DWCNT (K_L) than Zn(II), which could explain why more Pb(II) was adsorbed onto the surface of o-DWCNT at equilibrium even though its k_2 was smaller. Indeed, it is likely that Zn(II) adsorbs faster than Pb(II), but due to the higher interaction strength of Pb(II), this ion takes over the adsorption sites where Zn(II) was first located, as it has been observed by Tan *et al.*[25]. Compared to the literature, our k_2 results (Cd(II) = 1.10^{-6}, Cu(II) = 1.85.10^{-6}, Pb (II) = 9.10^{-6} and Zn(II) 1.3.10^{-6} g.mol^{-1}.min^{-1}) were a bit lower than Sitko *et al.* who found 9.79.10^{-5}, 2.52.10^{-4}, 4.34.10^{-5} and 7.19.10^{-4} g.mol^{-1}.min^{-1} for Cd(II), Cu(II), Pb(II) and Zn(II), respectively but the experimental conditions were different (Sitko *et al.*: pH = 5, MWCNT = 0.1 g.L^{-1}, metals = 5 mg.L^{-1})[26].

3.3. CNM type

First, concerning cumulative metal adsorption onto CNM, 3 groups could be distinguished (Figure 4, Kruskal-Wallis test among CNMs, p=0.012): one with a significantly higher adsorption level for GO (28.86 mmol.g^{-1}), another group with average adsorption for o-DWCNT, o-MWCNT and DWCNT (12.29,

11.43 and 13.41 mmol.g^{-1}, respectively) and a last one with a lower adsorption level for MWCNT and AC (5.64 and 4.50 mmol.g^{-1}, respectively). This result is consistent with the literature in mono-elemental conditions as demonstrated earlier with oxidised CNT adsorbing up to three times more metals than pristine CNT and GO from 5 to 30 times more[19]. These 3 groups seem to be established by the combination of several factors such as CNM SSA and level of oxidation.

The level of oxidation plays a key role in adsorption mechanisms. A first pattern can be seen for oxidized CNM with a high adsorption level with a mean of cumulative adsorption for oxidized CNM up to 17.52 mmol.g^{-1} and with a clear affinity sequence for metal adsorption for GO, o-DWCNT and o-MWCNT following Cu(II) = Pb(II) > Cd(II) = Zn(II) (14.08/12.28 > 1.17/1.33 mmol.g^{-1} for GO, 5.77/4.22 > 1.58/0.71 mmol.g^{-1} for o-DWCNT and 6.17/4.82 > 0.25/0.19 mmol.g^{-1} for o-MWCNT). A second pattern observed for pristine CNM displayed lower mean of cumulative adsorption with on average 7.85 mmol.g^{-1} and quasi-similar level of adsorption among metals with on average 3.35, 1.41 and 1.13 mmol.g^{-1} for all metals adsorbed on DWCNT, MWCNT and AC, respectively. As mentioned above, this could be related to different mechanisms of adsorption between oxidized materials (chemisorption) and pristine materials (physisorption).

The SSA is also a factor that could explain the differences of adsorption among CNM. Indeed, it has been observed in the literature that an increase in the diameter reduces the adsorption of metals on CNM surfaces, for CNM with a similar oxidation level[45,46]. Here, in the case of graphene oxide (GO), most interaction sites are present at the top and bottom faces (sites located at the edge may play a marginal role) that is why all the surface of that monolayer graphene is available for adsorption[47,48]. On the other hand, overall multilayer graphene and MWCNT tend to have lower SSA as their internal layers are little or not accessible by adsorbates[47]. Quite surprisingly, AC that displayed the highest SSA and a high level of O did not have a high sorption capacity. This observation has already been made before[20] and several hypotheses could be formulated to explain that phenomenon in our experiment. The first one would be related to the agglomeration status of the material in suspension[49] which is not

reflected by the SSA. However, in this case both AC and o-DWCNT (that has a similar O content, lower SSA but higher adsorption) had the same zeta potential (-33.9 ± 0.4 for AC and -35.4 ± 5.5 for o-DWCNT, at pH 5.5) which tends to invalidate this hypothesis. The second one relates to the nature of the O bearing functional groups and their accessibility[50]. The activation of carbon (for AC) leads to the formation of micropores possibly restricting the accessibility to the functional groups located within these pores as opposed to CNT which tend to display mesopores[51]. Additionally, from the Raman signature it can be seen that AC had a high degree of disorganisation (I_D/I_G AC= 1.21 vs I_D/I_G o-DWCNT = 0.23 Table S2) suggesting the presence of a large proportion of amorphous carbon also leading to a decrease of accessibility. Finally, some functional groups such as carboxylates and hydroxyls are known to bind more effectively cations than functionals groups such as carbonyls or lactones[21] suggesting that AC might have a higher proportion of these latter groups[52].

Very little is known about the possible transformations of CNM in the environment. Overall it seems that functionalised (oxidised) materials are more prone to degradation with some studies highlighting a possible degradation through enzymatic reactions or through biodegradation mediated by algae cells or bacteria[53,54]. Additionally, both reduction and oxidation of the surface were demonstrated. However, CNM remain among the most stable nanomaterials[53,54]. In parallel, it is very difficult to properly estimate the production of oxidised *vs.* pristine CNM. One could hypothesize from the few data available that there is on the market more or less the same proportion of these two types of materials. But there is a trend for increased market for oxidized CNM which are more easily dispersed in different matrices, but also have a better chemical purity as oxidation treatments are known to remove residual catalytic metals[55].

3.4. Organic Matter

Cumulative metal adsorption onto o-DWCNT decreased with OM concentration (Figure 5). It was significantly lower at 20 $mg.L^{-1}$ compared to the control with nearly 0 and 8.43 $mmol.g^{-1}$, respectively

446 (ANOVA 1 among MO conditions, p=0.020). However, OM addition did not modify adsorption of Cd(II)
447 and Zn(II) with similar values ranging from 0.5 to 1 mmol.g^{-1} whatever OM concentration. In contrast,
448 OM addition prevented Pb(II) and Cu(II) adsorption in a dose dependent manner leading to adsorption
449 values for Pb(II) ranging from 5.5 without OM to 1.7 and 0.35 mmol.g^{-1} with the addition of 10 and 20
450 mg.L^{-1} of OM, respectively and for Cu(II) ranging from 1.3 without OM to -0.9 and -2.9 mmol.g^{-1} with
451 the addition of 10 and 20 mg.L^{-1} of OM. One hypothesis explaining these different results could be that
452 OM adsorbs on the adsorption sites (-OH and -COOH) of o-DWCNT for which Pb(II) and Cu(II) have a
453 more pronounced affinity than Cd(II) and Zn(II) thereby preferentially reducing their adsorption.
454 Additionally, a second hypothesis could be that OM could also complex metallic ions (Pb(II) and Cu(II)
455 preferentially) which would then prevent their interactions with o-DWCNT surface. This last hypothesis
456 is further supported by Visual MINTEQ modelling (Stockholm Humic Model, fulvic acid, 0.01 mg DOC/L,
457 pH 7.5): the simulations show that 48% of reactive OM sites are occupied by Pb and 21% by Cu,
458 whereas Cd and Zn together account for <5% of complexed forms. This confirms the much higher
459 affinity of OM for Pb and Cu under our conditions and is fully consistent with the strong OM-driven
460 decrease in Pb and Cu adsorption, compared to the limited effect observed for Cd and Zn. Further FTIR
461 or XPS CNT surface analyses would be necessary to elucidate the interaction mechanisms, however
462 they require more concentrated samples. Some examples in the literature reported contrasting results,
463 with OM addition favouring Pb(II) and Cu(II) adsorption onto MWCNT[30,32]. These discrepancies could
464 be explained by the fact that pH conditions were different (Lin et al.[30] pH = 5 and Sheng et al[32]. pH =
465 4-10) leading to different interactions among CNT, OM and metals. In addition, Sheng et al. also
466 demonstrated a decrease of Cu adsorption onto MWCNT when pH > 7.5, supporting pH influence on
467 CNT/OM/metal interactions[32].

468 Surprisingly, adsorption results for Cu(II) were negative. These negative adsorption values for Cu(II) do
469 not indicate analytical artefacts but rather suggest that there were more Cu(II) in experimental units
470 with OM and o-DWCNT than in experimental units with OM without o-DWCNT, which in turn could
471 suggest that Cu(II) is better stabilized (possibly by OM) in the presence of o-DWCNT. The addition of

CNT in the medium modifies the interactions in this complex medium (OM + 4 metals) and could displace Cu equilibrium leading to less precipitated forms, especially in this experiment in which the pH was slightly higher (pH=7.5). However, dedicated experiments should be performed to better understand the complex mechanisms underlying these results.

In France, the great plains of intensive cultivation contain 1 to 2% of OM[33] which corresponds to the concentrations tested in our experiment. It thus suggests that metal adsorption would be limited in typical agricultural soils.

3.5. Soil solution

Despite the marked differences in pH (4.3 *vs* 5.7) and ionic strength between the two soil solutions, adsorption patterns remained very similar. The cumulative metal adsorption onto o-DWCNT did not differ between soil types (3.15 and 3.41 $mmol \cdot g^{-1}$ for soils 2.1 and 6S, respectively, Kruskal-Wallis between the 2 soil types: p=0.369), nor among metals, with comparable values for Cd(II), Cu(II), Pb(II) and Zn(II) in both solutions (on average 1.12, 0.33, 0.60 and 1.10 $mmol.g^{-1}$ for Cd(II), Cu(II), Pb(II) and Zn(II), respectively for 2.1 soil solution and 1.14, 0.91, 0.20 and 1.16 $mmol.g^{-1}$, respectively for Cd(II), Cu(II), Pb(II) and Zn(II) for 6S soil solution; Figure S7; Kruskal-Wallis among all conditions: p=0.400). When compared with adsorption in ultrapure water at similar pH (1.96 $mmol \cdot g^{-1}$ at pH 5), these values fall within the same range and show no preferential uptake, indicating that soil-borne dissolved components did not substantially alter metal–CNT interactions under our conditions.

This limited variation suggests that pH-driven surface charge effects dominate over competition with background ions. Although the ionic strengths of soil 2.1 and 6S (0.0026 and 0.0046 $mol \cdot L^{-1}$, respectively) indicate the presence of divalent cations such as Ca^{2+} and Mg^{2+}, their concentrations remain too low to significantly compete with trace metals for adsorption sites on o-DWCNT.

The higher variability observed in this experiment likely reflects metal precipitation induced by soil-solution constituents. This was confirmed by the negative controls (without o-DWCNT), where initial Cu(II) and Pb(II) concentrations decreased to 0.93 mM in soil 2.1, but dropped further to 0.45 and 0.11 mM, respectively, in soil 6S—deviating substantially from the nominal 1 mM. The granulometry of upper agricultural soil horizons in France is a mix between loamy and clayey soil[33] (somewhere in between the two soils used in this experiment) suggesting that the adsorption behaviour of metals on the surface of CNT should be similar whatever soil granulometry, with similar adsorption levels of Cd(II), Cu(II), Pb(II) and Zn(II).

4. General conclusion

The results obtained here provide a significant contribution towards a better understanding of the interactions among contaminants in natural environments and their impacts on both transfer and toxicity of such contaminants. They also demonstrate the importance of taking into account ionic precipitation when investigating sorption equilibrium in aqueous medium (*e.g.* about 10% of precipitation at pH 8 for Pb at 1 mM or about 20% for Cu at 2.5 mM at pH 7), which is rarely done. Regarding the average agricultural soil properties such as soil pH (pH = 5.8), OM concentration (1-2%), granulometry (equilibrium between loamy and clayey soils) and CNM/metal ratio (with metals in excess in comparison with CNM), the results of this work suggest equivalent adsorption of Cd(II), Cu(II), Pb(II) and Zn(II) on the surface of CNT in our experimental conditions, with rather low values (1-2 $mmol.g^{-1}$). Also, Cu and Pb adsorption could decrease with higher OM concentration. According to these results, pH and OM are the two environmental parameters that most influence the adsorption behaviour of metals on the surface of CNT together with the level of CNT oxidation and in particular the proportion of carboxylic groups. In addition, many compounds such as pesticides, herbicides and others are simultaneously present in agrosystems, compounds which could also adsorb onto CNT[56] and modify metal adsorption behaviour. While our study provides a comprehensive assessment under

environmentally relevant conditions, it is inherently constrained by the low concentrations typical of natural systems, which prevent the use of characterization techniques such as FTIR or SEM/EDS to better highlight the nature of metal-CNM interactions. These methodological limitations reflect real environmental scenarios but also highlight the need for complementary mechanistic investigations. Additionally, future studies could further assess how these processes evolve in real soil matrices with contrasting mineralogy, OM quality, and ageing effects, in order to capture the full complexity of metal–CNM interactions under field conditions.

Acknowledgements

The authors would like to acknowledge the Région Occitanie, Toulouse Federal University (under research programme NANOMETAGRO), and EC2CO program CARBOSTRESS (CNRS-INSU) for their funding support. Part of this work was funded by the European Union (ERC LEAPHY, 101041729). We also thank Frédéric Candaudap and Frédéric Julien, R&D engineers on the FBiI (ICP-AES) and PAPC (physico-chemical analysis) platforms of Centre de Recherche sur la Biodiversité et l'Environnement. Finally, the authors thank Marie-Claire Barthélémy, Roman Teisserenc, Anne-Marie Galibert, Brigitte Soula, Joséphine Leflaive and Mathilde Clavier for their valuable technical help and scientific discussions.

Author contributions: CRediT

Mathieu Leroy: Conceptualization, Data curation, Formal analysis, Investigation, Writing original draft. **Astrid Avellan**: Resources, Validation, Writing – review and editing. **Morgan Legnani**: Methodology. **Emmanuel Flahaut**: Conceptualization, Funding acquisition, Supervision, Validation, Writing – review and editing. **Camille Larue**: Conceptualization, Funding acquisition, Project administration, Supervision, Validation, Writing – original draft

BIBLIOGRAPHY

1. Padmanabhan, N. T., Gayathri, K., Thomas, R. M. & John, H. ZnO/Mo2TiC2 MXene nanohybrids for enhanced solar-driven photocatalytic degradation of tetracycline and organic pollutants in contaminated water. *Energy Environ. Sustain.* **1**, 100042 (2025).

2. Qin, X., Cui, H. & Zhou, Q. Physisorption behaviors of organochlorine pesticides on the InP3 monolayer from theoretical insight. *ACS Omega* **8**, 32168–32175 (2023).

3. Liu, R. *et al.* Innovative amorphous calcium carbonate for superior anionic dye adsorption towards near-zero discharge. *Sep. Purif. Technol.* **361**, **part**, 131349 (2025).

4. Belcaid, A., Beakou, B. H., Bouhsina, S. & Anouar, A. Biosorption of cobalt and chromium from wastewater using manganese dioxide and iron oxide nanoparticles loaded on cellulose-based biochar: Modeling and optimization with machine learning (artificial neural network). *Int. J. Biol. Macromol.* **282**, 136855 (2024).

5. Belcaid, A., Beakou, B. H., Bouhsina, S. & Anouar, A. Insight into adsorptive removal of methylene blue, malachite green, and rhodamine B dyes by cassava peel biochar (Manihot esculenta Crantz) in single, binary, and ternary systems: competitive adsorption study and theoretical calculations. *Biomass Convers. Biorefinery* **14**, 7783–7806 (2024).

6. Xie, L. *et al.* An efficient voltammetric sensing platform for trace determination of Norfloxacin based on nanoplate-like α-zirconium phosphate/carboxylated multiwalled carbon nanotube nanocomposites. *Microchem. J.* **206**, 111451 (2024).

7. Organization, W. H. *Guidelines for drinking-water quality: fourth edition incorporating the first and second addenda*. (2022).

8. European Commission. *Commission Regulation (EU) 2023/915 of 25 April 2023 on maximum levels for certain contaminants in food and repealing Regulation (EC) No 1881/2006 (Text with EEA relevance)*. (2023).

9. Hou, D. *et al.* Global soil pollution by toxic metals threatens agriculture and human health. *Science (80-.).* **388**, 316–321 (2025).

10. Ondrasek, G. *et al.* Metal contamination – a global environmental issue: sources, implications & advances in mitigation. *RSC Adv.* **15**, 3904–3927 (2025).

11. Gottschalk, F., Sun, T. & Nowack, B. Environmental concentrations of engineered nanomaterials: Review of modeling and analytical studies. *Environ. Pollut.* **181**, 287–300 (2013).

12. Jones, A. *et al. The State of Soil in Europe*. (2012).

13. Holden, P. A. *et al.* Evaluation of exposure concentrations used in assessing manufactured nanomaterial environmental hazards: are they relevant? *Environ. Sci. Technol.* **48**, 10541–10551 (2014).

14. Butt, B. Z. & Naseer, I. Nanofertilizers. in *Nanoagronomy* (ed. Javad, S.) 125–152 (Springer, 2020). doi:10.1007/978-3-030-41275-3_8.

15. Paramo, L. A., Feregrino-Pérez, A. A., Guevara, R., Mendoza, S. & Esquivel, K. Nanoparticles in agroindustry: applications, toxicity, challenges, and trends. *Nanomaterials* **10**, 1654 (2020).

16. Perreault, F., Fonseca de Faria, A. & Elimelech, M. Environmental applications of graphene-based nanomaterials. *Chem. Soc. Rev.* **16**, 5861–5896 (2015).

17. Rai, P. K., Lee, S. S., Zhang, M., Tsang, Y. F. & Kim, K.-H. Heavy metals in food crops: Health risks, fate, mechanisms, and management. *Environ. Int.* **125**, 365–385 (2019).

18. EUR-LEX. Council Directive of 12 June 1986 on the protection of the environment, and in particular of the soil, when sewage sludge is used in agriculture (86/278/EEC). https://eur-lex.europa.eu/legal-content/EN/TXT/?uri=CELEX%3A01986L0278-20180704 (1986).

19. Leroy, M., Flahaut, E. & Larue, C. Carbon based nanomaterial interactions with metals and

592 metalloids in terrestrial environment: a review. *Carbon N. Y.* **206**, 325–339 (2023).

593 20. Aigbe, U. O. & Osibote, O. A. Carbon derived nanomaterials for the sorption of heavy metals
594 from aqueous solution: A review. *Environ. Nanotechnology, Monit. Manag.* **16**, 100578
595 (2021).

596 21. Chandran, D. G., Muruganandam, L. & Biswas, R. A review on adsorption of heavy metals from
597 wastewater using carbon nanotube and graphene-based nanomaterials. *Environ. Sci. Pollut.*
598 *Res.* **30**, (2023).

599 22. Ding, C. *et al.* Competitive sorption of Pb(II), Cu(II) and Ni(II) on carbonaceous nanofibers: A
600 spectroscopic and modeling approach. *J. Hazard. Mater.* **313**, 253–261 (2016).

601 23. Salam, M. A., Al-Zhrani, G. & Kosa, S. A. Simultaneous removal of copper(II), lead(II), zinc(II)
602 and cadmium(II) from aqueous solutions by multi-walled carbon nanotubes. *Comptes Rendus*
603 *Chim.* **15**, 398–408 (2012).

604 24. Alimohammady, M., Jahangiri, M., Kianib, F. & Tahermansourib, H. Highly efficient
605 simultaneous adsorption of Cd(ii), Hg(ii) and As(iii) ions from aqueous solutions by
606 modification of graphene oxide with 3-aminopyrazole: central composite design optimization.
607 *New J. Chem.* **41**, 8905–8919 (2017).

608 25. Tan, P., Hu, Y. & Bi, Q. Competitive adsorption of Cu2+, Cd2+ and Ni2+ from an aqueous
609 solution on graphene oxide membranes. *Colloids Surfaces A Physicochem. Eng. Asp.* **509**, 56–
610 64 (2016).

611 26. Sitko, R. *et al.* Adsorption of divalent metal ions from aqueous solutions using graphene oxide.
612 *Dalt. Trans.* **42**, 5682–5689 (2013).

613 27. Li, Y.-H. *et al.* Competitive adsorption of Pb2+, Cu2+ and Cd2+ ions from aqueous solutions by
614 multiwalled carbon nanotubes. *Carbon N. Y.* **41**, 2787–2792 (2003).

615 28. Lu, C., Liu, C. & Su, F. Sorption kinetics, thermodynamics and competition of Ni2+ from
616 aqueous solutions onto surface oxidized carbon nanotubes. *Desalination* **249**, 18–23 (2009).

617 29. Xiao, B. & Thomas, K. M. Competitive adsorption of aqueous metal ions on an oxidized
618 nanoporous activated carbon. *Langmuir* **20**, 4566–4578 (2004).

619 30. Lin, D. *et al.* Surface-bound humic acid increased Pb2+ sorption on carbon nanotubes. *Environ.*
620 *Pollut.* **167**, 138–147 (2012).

621 31. Tian, X. *et al.* Effect of humic acids on physicochemical property and Cd(II) sorption of
622 multiwalled carbon nanotubes. *Chemosphere* **89**, 1316–1322 (2012).

623 32. Sheng, G. *et al.* Adsorption of copper(II) on multiwalled carbon nanotubes in the absence and
624 presence of humic or fulvic acids. *J. Hazard. Mater.* **178**, 333–340 (2010).

625 33. GIS Sol, -. *L'état des sols de France*. (2011).

626 34. De Troyer, I., Merckx, R., Amery, F. & Smolders, E. Factors controlling the dissolved organic
627 matter concentration in pore waters of agricultural soils. *Vadose Zo. J.* **13**, 1–9 (2014).

628 35. Ren, X., Chen, C., Nagatsu, M. & Wang, X. Carbon nanotubes as adsorbents in environmental
629 pollution management: A review. *Chem. Eng. J.* **170**, 395–410 (2011).

630 36. Moradi, O. The removal of ions by functionalized carbon nanotube: equilibrium, isotherms
631 and thermodynamic studies. *Chem. Biochem. Eng. Q.* **25**, 229–240 (2011).

632 37. Vuković, G. D. *et al.* Removal of cadmium from aqueous solutions by oxidized and
633 ethylenediamine-functionalized multi-walled carbon nanotubes. *Chem. Eng. J.* **157**, 238–248
634 (2010).

635 38. Chen, P. H., Hsu, C.-F., Tsai, D. D., Lu, Y.-M. & Huang, W.-J. Adsorption of mercury from water
636 by modified multi-walled carbon nanotubes: adsorption behaviour and interference
637 resistance by coexisting anions. *Environ. Technol.* **35**, 1935–44 (2014).

638 39. Gupta, A., Vidyarthi, S. R. & Sankararamakrishnan, N. Enhanced sorption of mercury from
639 compact fluorescent bulbs and contaminated water streams using functionalized multiwalled
640 carbon nanotubes. *J. Hazard. Mater.* **274**, 132–44 (2014).

641 40. Zhang, Z., Pfefferle, L. & Haller, G. L. Characterization of functional groups on oxidized multi-
642 wall carbon nanotubes by potentiometric titration. *Catal. Today* **249**, 23–29 (2015).

643 41. Fabian, C. *et al.* GEMAS: Spatial distribution of the pH of European agricultural and grazing
644 land soil. *Appl. Geochemistry* **48**, 207–216 (2014).

645 42. de Soto, I. S., Zamanian, K., Urmeneta, V., Enrique, H. & Iñigo, A. 25 years of continuous
646 sewage sludge application vs. mineral fertilizers on a calcareous soil affected pH but not soil
647 carbonates. *Front. Soil Sci.* **2**, (2022).

648 43. Davodi, B. & Jahangiri, M. Determination of optimum conditions for removal of As (III) and As
649 (V) by polyaniline/polystyrene nanocomposite. *Synth. Met.* **194**, 97–101 (2014).

650 44. European Commission. Council Directive of 12 June 1986 on the protection of the
651 environment, and in particular of the soil, when sewage sludge is used in agriculture
652 (86/278/EEC). https://eur-lex.europa.eu/legal-content/FR/TXT/?uri=CELEX%3A01986L0278-
653 20180704 (1986).

654 45. Lu, C., Chiu, H. & Liu, C. Removal of zinc(II) from aqueous solution by purified carbon
655 nanotubes: kinetics and equilibrium studies. *Ind. Eng. Chem. Res.* **45**, 2850–2855 (2006).

656 46. Lu, C. & Chiu, H. Adsorption of zinc(II) from water with purified carbon nanotubes. *Chem. Eng.*
657 *Sci.* **61**, 1138–1145 (2006).

658 47. Sitko, R., Zawisza, B. & Malicka, E. Graphene as a new sorbent in analytical chemistry. *Trends*
659 *Anal. Chem.* **51**, 33–43 (2013).

660 48. Zhao, J., Wang, Z., White, J. C. & Xing, B. Graphene in the aquatic environment: adsorption,

dispersion, toxicity and transformation. *Environ. Sci. Technol.* **48**, 9995–10009 (2014).

49. Rodríguez, C., Briano, S. & Leiva, E. Increased adsorption of heavy metal ions in multi-walled carbon nanotubes with improved dispersion stability. *Molecules* **25**, 3106 (2020).

50. Yang, X. *et al.* Surface functional groups of carbon-based adsorbents and their roles in the removal of heavy metals from aqueous solutions: A critical review. *Chem. Eng. J.* **15**, 608–621 (2019).

51. Qiu, C., Jiang, L., Gao, Y. & Sheng, L. Effects of oxygen-containing functional groups on carbon materials in supercapacitors: A review. *Mater. Des.* **230**, 111952 (2023).

52. Kouassi Brou, G. *et al.* Caractéristiques physico-chimiques du charbon de pyrolyse de coques de noix d'anacarde et des charbons actifs qui en sont dérivés. *Tech. l'ingénieur* **82**, 17–24 (2019).

53. Peng, Z. *et al.* Advances in the application, toxicity and degradation of carbon nanomaterials in environment: A review. *Environ. Int.* **134**, 105298 (2020).

54. Lowry, G. V., Gregory, K. B., Apte, S. C. & Lead, J. R. Transformations of nanomaterials in the environment. *Environ. Sci. Technol.* **46**, 6893–6899 (2012).

55. Bortolamiol, T. *et al.* Double-walled carbon nanotubes: Quantitative purification assessment, balance between purification and degradation and solution filling as an evidence of opening. *Carbon N. Y.* **78**, 79–90 (2014).

56. Pyrzynska, K. Carbon nanotubes as sorbents in the analysis of pesticides. *Chemosphere* **83**, 1407–1413 (2011).

683 **Figures**

684

685 **Figure 1**

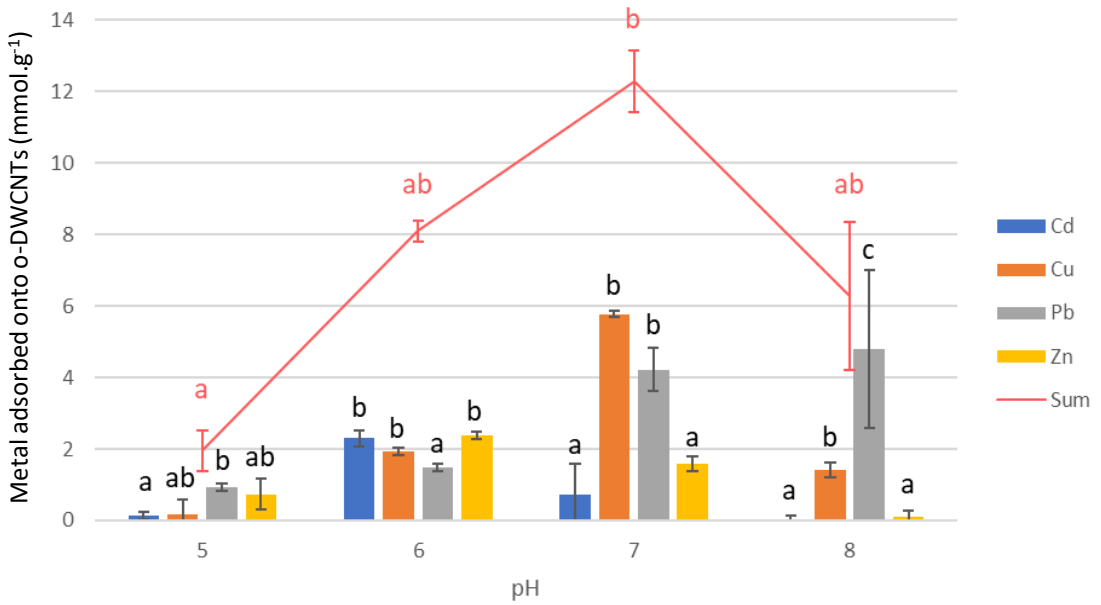

686

687 *Figure 1: Metal (Cd, Cu, Pb and Zn) adsorbed onto o-DWCNT depending on the pH (o-DWCNT concentration: 10 mg.L^{-1}, metal*
688 *concentrations: 1 mM. Contact time: 3 hours, temperature: 18.3 ± 0.9 °C). Same lowercase letters indicate treatments that do*
689 *not differ significantly following a Kruskal-Wallis test. Statistical analysis has been performed within a pH value except for the*
690 *sum (n=5).*

691

692

693 **Figure 2**

694

A

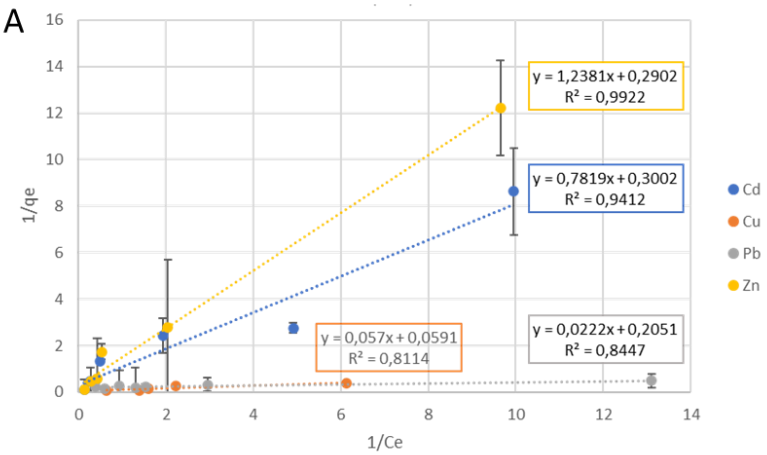

B

	Intercept	Slope	q_{max}	q_{exp}	K_L	R_L	R^2
Cd	0.30	0.08	3.33	1.24	3.84	0.03	0.94
Cu	0.06	0.06	16.92	13.48	1.04	0.09	0.81
Pb	0.21	0.02	4.88	5.55	9.24	0.01	0.84
Zn	0.29	1.24	3.45	1.49	0.23	0.30	0.99

695

696 *Figure 2: Multi-metallic Langmuir linear isotherm, all data points include error bars; for some conditions the variability is very*
697 *small, resulting in error bars that are hidden beneath the symbols (A) and Langmuir adsorption isotherm constants (B) for Cd,*
698 *Cu, Pb and Zn with o-DWCNT (o-DWCNT concentration: 10 mg.L^{-1}, metal concentrations for isotherm modelling: 0.1-4 mM for*
699 *Cd and Zn, 0.2-4 mM for Pb and 0.1-2.5 mM for Cu, pH: 7, contact time: 3 hours, temperature: 18.3 ± 0.9 °C), qe: metal quantity*
700 *adsorbed onto o-DWCNT (mmol.g^{-1}), Ce: equilibrium aqueous concentration (mM), q_{max}: maximal quantity of metal adsorbed*
701 *onto o-DWCNT at the equilibrium calculated by Langmuir model (mmol.g^{-1}), q_{exp}: experimental quantity of metal adsorbed*
702 *onto o-DWCNT at the equilibrium (mmol.g^{-1}), K_L= adsorption equilibrium constant, R_L : separation factor, R^2 : correlation*
703 *coefficient)*

704

705

Figure 3

A

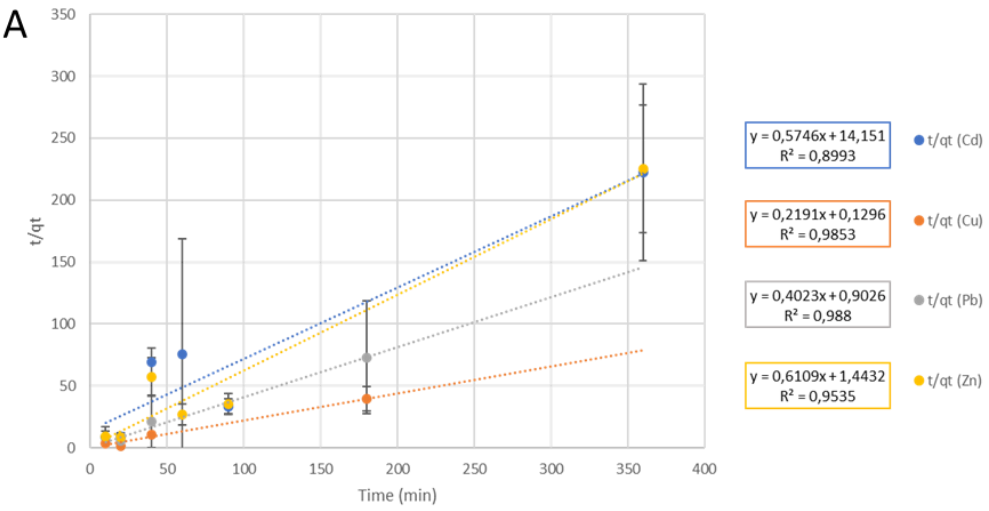

B

	Intercept	Slope	q_e	K_2	R^2
Cd	14.19	0.57	1.75	0.02	0.90
Cu	0.13	0.22	4.55	0.37	0.90
Pb	0.90	0.40	2.50	0.18	0.99
Zn	1.44	0.61	1.64	0.26	0.95

Figure 3: Multi-metallic non-linear pseudo-second order (A) and pseudo-second order constants (B) for Cd, Cu, Pb and Zn with o-DWCNT (o-DWCNT concentration: 10 mg.L^{-1}, metal concentrations: 1 mM for Cd, Cu, Pb and Zn, pH: 7, contact time: 10 to 360 min^{-1}, temperature: 18.3 ± 0.9 °C, qe: metal quantity adsorbed onto o-DWCNT calculated by pseudo-second order model (mmol.g^{-1}), qt: total quantity of metals adsorbed onto o-DWCNT, k_2= constant rate of the pseudo-second-order (g.mmol.min^{-1}), R^2 : correlation coefficient)

Figure 4

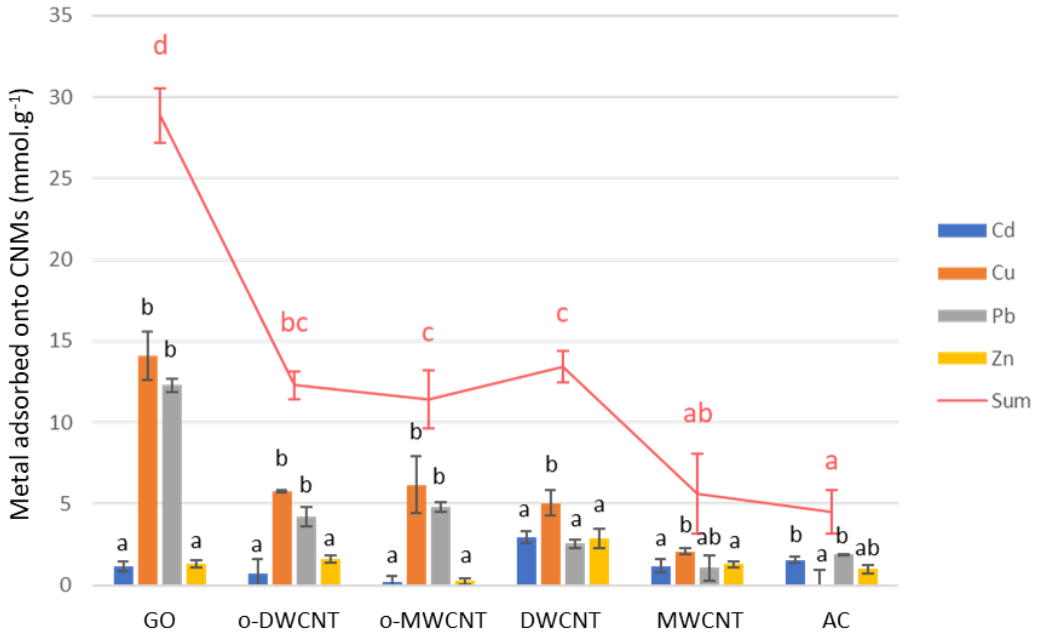

Figure 4: Metals (Cd, Cu, Pb and Zn) adsorbed onto different carbon based nanomaterials: graphene oxide (GO), oxidized double-walled CNT (o-DWCNT), oxidized multi-walled CNT (o-MWCNT), pristine double-walled CNT (DWCNT), pristine multi walled CNT (MWCNT) and activated carbon (AC) using a multi-metallic solution (CNM concentration: 10 mg.L^{-1}, metal concentrations: 1 mM, pH: 7, contact time: 3 hours, temperature: 18.3 ± 0.9 °C). Same lowercase letters indicate treatments that do not differ significantly within a CNM type following 1-way ANOVA or among CNM following a Kruskal-Wallis test (p-value > 0.05; n=5).

Figure 5

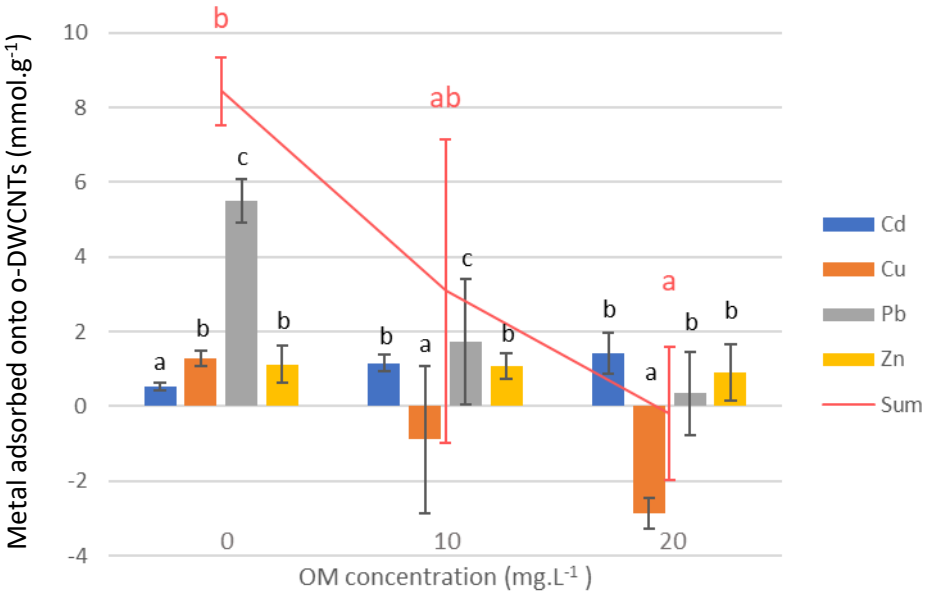

Figure 5: Metals (Cd, Cu, Pb and Zn) adsorbed onto o-DWCNT using a multi-metallic solution according to OM concentration in the medium (o-DWCNT concentration: 10 mg.L^{-1}, metal concentrations 1 mM, pH: 7.5, contact time: 3 hours, temperature: 18.3 ± 0.9 °C, OM: Organic Matter). Same lowercase letters indicate treatments that do not differ significantly following 1-way ANOVA. ANOVA was performed within a same OM concentration or among MO conditions (p-value > 0.05; n=5)